Supporting Information

Highly Selective Transfer Hydrogenation of Functionalised Nitroarenes Using Cobalt-based Nanocatalysts

Rajenahally V. Jagadeesh, Debasis Banerjee, Percia B. Arockiam, Henrik Junge, Kathrin Junge, Marga-Martina Pohl, Jörg Radnik, Angelika Brückner, Matthias Beller*

Leibniz-Institut für Katalyse e. V. an der Universität Rostock, Albert-Einstein-Str. 29a,18059 Rostock, Germany.
E-mail: Matthias.Beller@catalysis.de;
Fax: (+49)-381-1281-51113; Phone: (+49)-381-1281-113

Table of Contents:

S1. Procedure for the preparation of cobalt oxide-based nanocatalysts

All chemicals used for the preparation of catalysts are commercially available..The vulcan XC72R was purchased form Cabot Limited. The pyrolsis experiments were carried out in Centurion™ Neytech Qex Vacuum Furnace. The tyipcal procedure for the preparation of the active catalyst is described as follows: A mixture of $Co(OAc)_2.4H_2O$ (corresponds to 3 wt% Co) and 1,10-phenanthroline (Co:phenanthroline = 1:2 mole ratio) in ethanol was stirred for 20-30 minutes at room temperature. Then, vulcan XC72R carbon powder was added and the whole reaction mixture was stirred at 60 °C for 5-6 hours. The reaction mixture was cooled to room temperature and ethanol was removed slowely under vacuum. The remaining solid sample obtained was dried at 60 °C for 12 hours. The dried sample was grinded to a powder. Then, the grinded powder was pyrolyzed at 800 °C for 2 hours in the gradiant of 25 ^{0}C per minut in argon atmosphere and cooled to room temperature.

Elemental analysis of Co-Phenanthroline/C (Wt%): C = 89.68, H = 0.199, N = 2.70, Co = 3.05.

XPS data of Co-Phenanthroline/C (Atom%): C = 92.38, N = 2.80, Co = 0.61, O = 4.02

S2. TEM measurements and images of the cobalt oxide-based nanocatalysts

The TEM measurements were performed at 200kV on a JEM-ARM200F (JEOL) which is aberration corrected by a CESCOR (CEOS) for the STEM applications. The microscope is equipped with a JED-2300 (JEOL) EDXS spectrometer for chemical analysis. The HAADF imaging was performed with spotsize 6c and a 40µm condenser aperture. The sample was deposited on a holey carbon supported grid mesh 300 and transferred to the microscope. To image the full size spectra of Co_3O_4 particles, High Angle Annular Dark Field (HAADF) at a Cs corrected microscope was used. With a conventional TEM it was not possible to image the smallest particles due to the weak contrast. As shown in Fig. S1, in the catalyst contains mainly small particles of 2-10 nm in size. By EDXS analysis, cobalt along with oxygen was detected in such particles (Fig. S2), suggesting that they consist of CoO and/or Co_3O_4. This agrees very well with the XRD pattern showing only very weak signals of CoO and Co_3O_4(Fig. S7). Due to their small size, such particles are hardly visible by XRD.

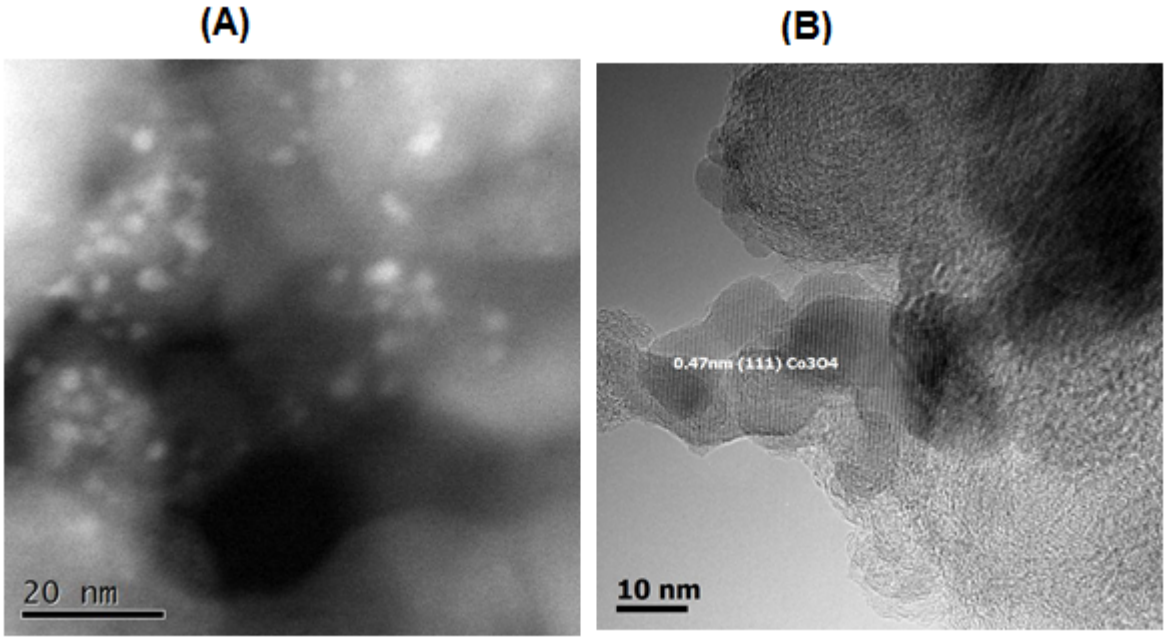

Fig.S1-STEM-HAADF of Co_3O_4-NGr/ catalysts

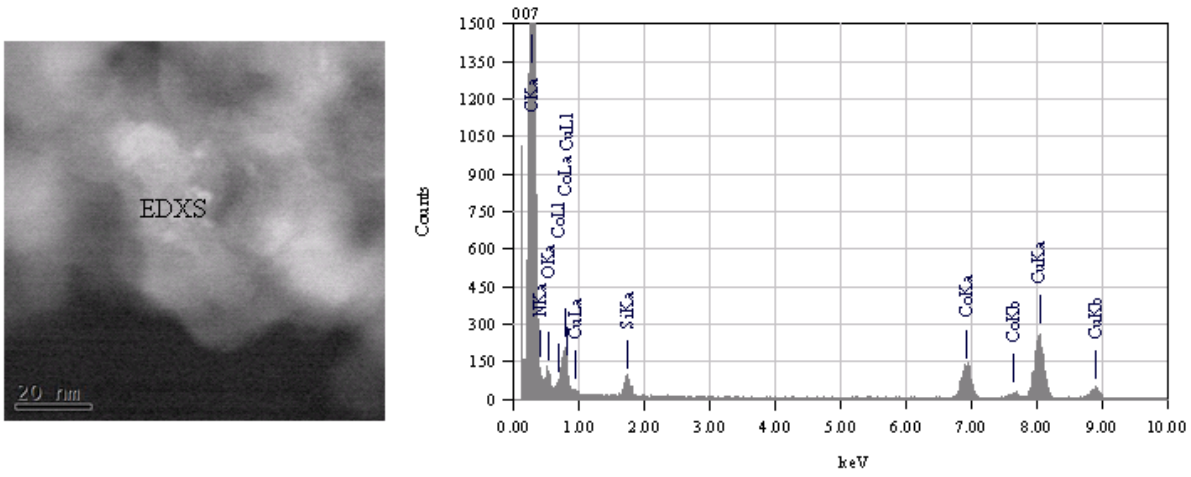

Fig. S2. EDX analysis (right) of the particle indicated in the left plot.

Besides the small particles shown in Fig. S1 and S2, there are also a few larger particles and agglomerates in a range of 20-80 nm and occasionally even larger structures up to 800 nm. As an example, one of these structures is shown in Fig. S3. EDXS mapping shows clearly that Co is concentrated in the core of such particles, while oxygen is enriched in the shell. Thus, those larger particles might consist of a Co core and a CoO and/or Co_3O_4 shell. In the XRD pattern (Fig. S7) these particles, though much less abundant than the small particles shown in Fig. S1, give rise to the sharp reflections for metallic Co. This is due to their much larger size and higher crystallinity.

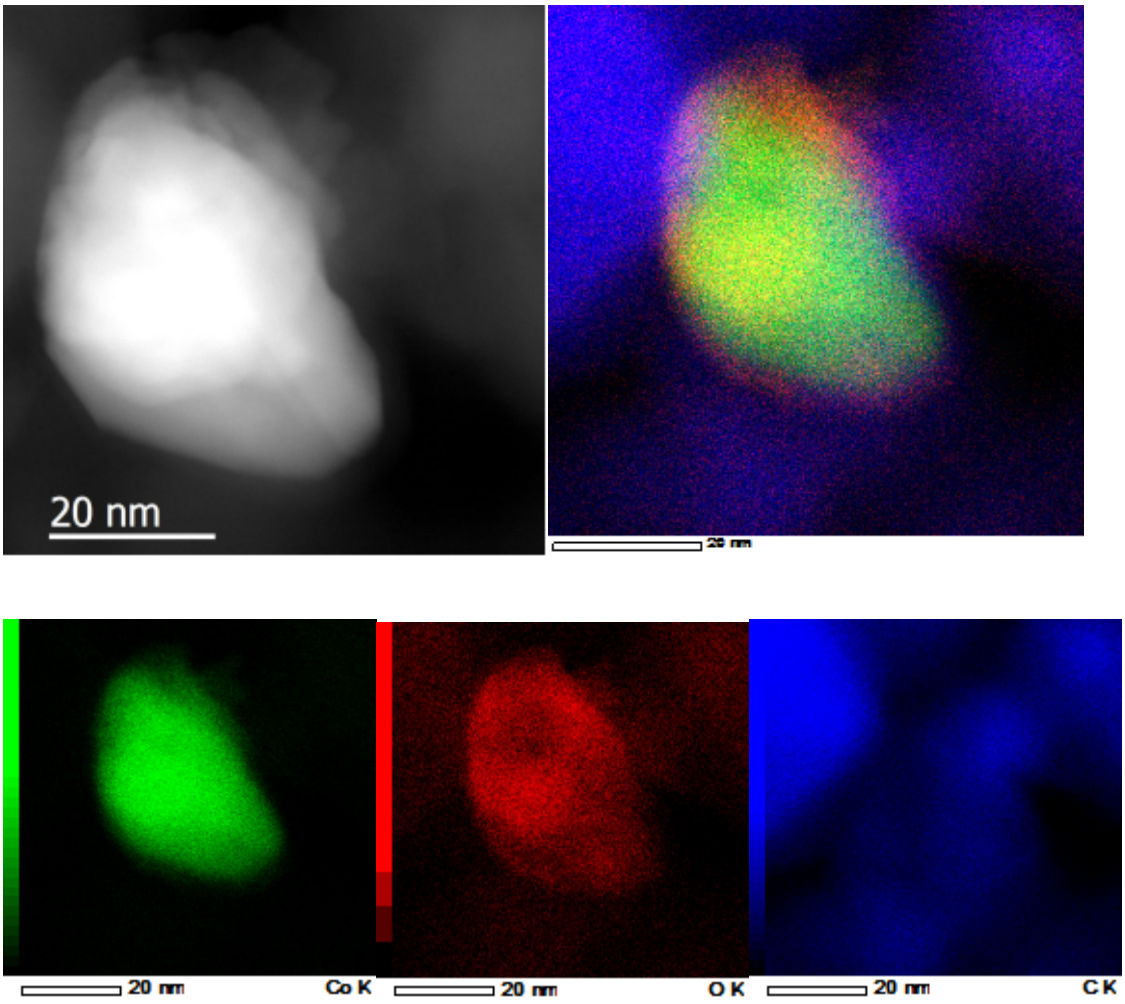

Fig. S3. Micrograph and elemental mapping (green: Co; red: oxygen; blue: carbon (from the grid)

S3. XPS Measurements and data of cobalt oxide-based nanocatalysts

To obtain further insight into the structure of the catalyst surface and especially into the role of nitrogen coming from the organic ligand, XPS investigations of N and Co species were carried out. Interestingly, three distinct peaks are observed in the N1s spectra of the Co_3O_4-NGr/C-catalyst with an electron binding energy of 399.0 eV, 400.8 eV and 402.3 eV (Fig. S4). The lowest binding energy peak can be attributed to pyridine-type nitrogen, which is bound to a metal ion.[S1] The electron binding energy of 400.8 eV is characteristic for pyrrole-type nitrogen contributing two electrons to the carbon matrix. It is bound to a hydrogen atom. Such types of nitrogen are found after the carbonization of nitrogen-containing organic materials.[S2] Finally, the small peak at 402.3 eV is typical for ammonium species like NH_4^+ or R-NH_3^+.[S3] The ratio between all Co atoms and all N atoms in the near surface region is 1:4.7. Deconvolution reveals that around 64% of all N atoms are bound to the metal ions.

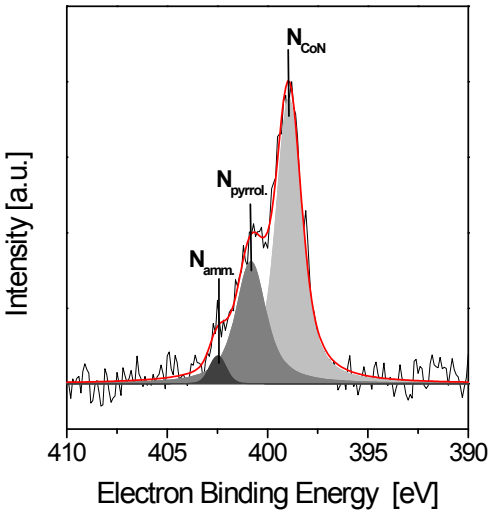

Fig. S4. N1s spectrum of the catalyst. The different N1s state are labelled: N_{CoN} N bound to Co; $N_{pyrrol.}$: pyrrolic N; $N_{amm.}$: N of ammonium species

In the cobalt region, only peaks characteristic for oxidic Co are found (Fig. S5) with the typical binding energy of 780.4 eV of the Co2$p_{3/2}$ and 795.3 eV of the Co 2$p_{1/2}$ electrons are found. Additionally, the satellite peaks at 786.7 eV and 802.8 eV are charecteristic for oxidic Co. This agrees very well with TEM results, which suggest that the very small particles of 2-10 nm are oxidic (in line with XRD) and the bigger particles contain a Co core and a cobalt oxide shell. In the literature[S4] it is discussed, that CoO on the surface is not stable and therefore oxidized to Co_3O_4. Thus, it can be concluded that the surface of all Co-containing particles in the catalyst consists of Co_3O_4 while CoO and Co (reflected by XRD) might be enriched in the bulk.

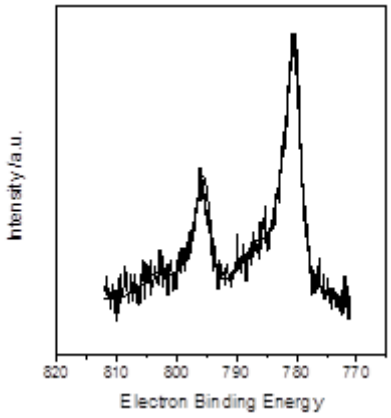

Fig. S5. Co2p spectrum of the catalyst with the typical features of Co_3O_4

S4. EPR measurements and data

EPR spectra were recorded in X-band at 80 K and 290 K on a Bruker EMX CW-micro spectrometer equipped with an ER 4119HS-WI high-sensitivity cavity and a variable temperature control unit (microwave power: 6.64 mW, modulation frequency: 100 kHz, modulation amplitude: 1 G). The EPR spectrum of the active catalyst contains a broad signal at g = 2.12 (Fig. S6). The intensity of this signal increases slightly with rising temperature, which is characteristic for antiferromagnetic Co_3O_4 particles. The Neel temperature T_N above which bulk Co_3O_4 becomes paramagnetic is below 40 K.[S5,S6] Previously it was found that the temperature dependence of the EPR signal intensity reflects very sensitively the onset of anti-ferromagnetic ordering in Co_3O_4 and also in other antiferromagnetic oxide materials already well above T_N.[S7] In bulk Co_3O_4 the EPR intensity increased gradually up to 150 K and then remained constant up to 250 K before it started decreasing.[S6] The observed intensity behaviour in Fig. S6 is exactly in line with these previous results.

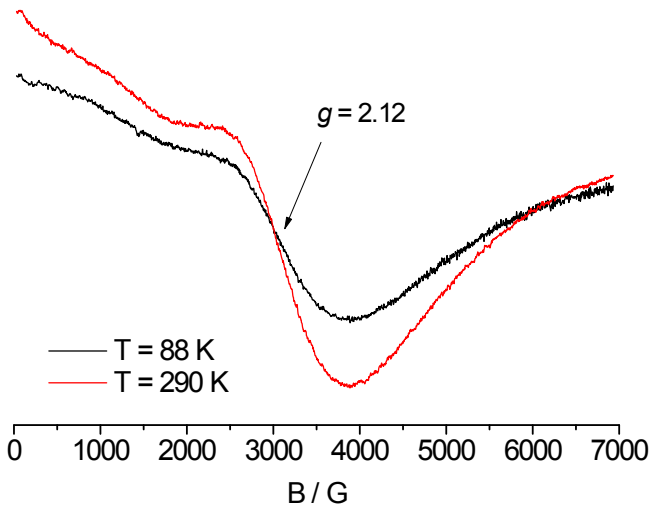

Figure S6. EPR spectra of the active cobalt catalyst recorded at 88 and 290 K.

The EPR signal at g = 2.12 is superimposed on a second very broad anisotropic signal, the positive lobe of which is cut off at B = 0. This suggests that the magnetic properties are not exactly the same for each particle. The reason may be different particle sizes (see above) and/or replacement of O by N in the coordination of Co (as observed by XPS above). In

contrast to Co_3O_4, CoO is not expected to contribute to the EPR spectrum since CoO is antiferromagnetic below $T_N \approx 293K$[S8] and thus EPR silent. Metallic Co is ferromagnetic up to a Curie temperature of 1120 °C[S9] and could in principle cause a ferromagnetic resonance signal, the intensity of which does not depend on temperature between 88 and 290 K. Such signal is not seen in Fig. S6 (possibly due to the very low amount of metallic particles in the catalyst as suggested by TEM), however, it cannot be excluded that it contributes to some extend to the background of the EPR spectrum.

S5. XRD measurements and data

The XRD powder pattern was recorded on a Stoe STADI P diffractometer, equipped with a linear Position Sensitive Detector (PSD) using Cu Kα radiation (λ = 1.5406 Å). Processing and assignment of the powder patterns was done using the software WinXpow (Stoe) and the Powder Diffraction File (PDF) database of the International Centre of Diffraction Data (ICDD). The powder pattern of the catalyst shows two sharp peaks characteristic for metallic Co (Fig. S1) at 2Θ = 44.16° and 51.42° besides weak reflections at 2Θ = 36.35°, 36.89°, 42.47 and 61.52°. The peaks at 36.35°, 42.47°and 61.52° confirm the existence of CoO, whereas the peak at 36.89° and the features around 59° 65.5° point to small Co_3O_4 particles just above the detection limit of XRD, which were confirmed by TEM (see above).

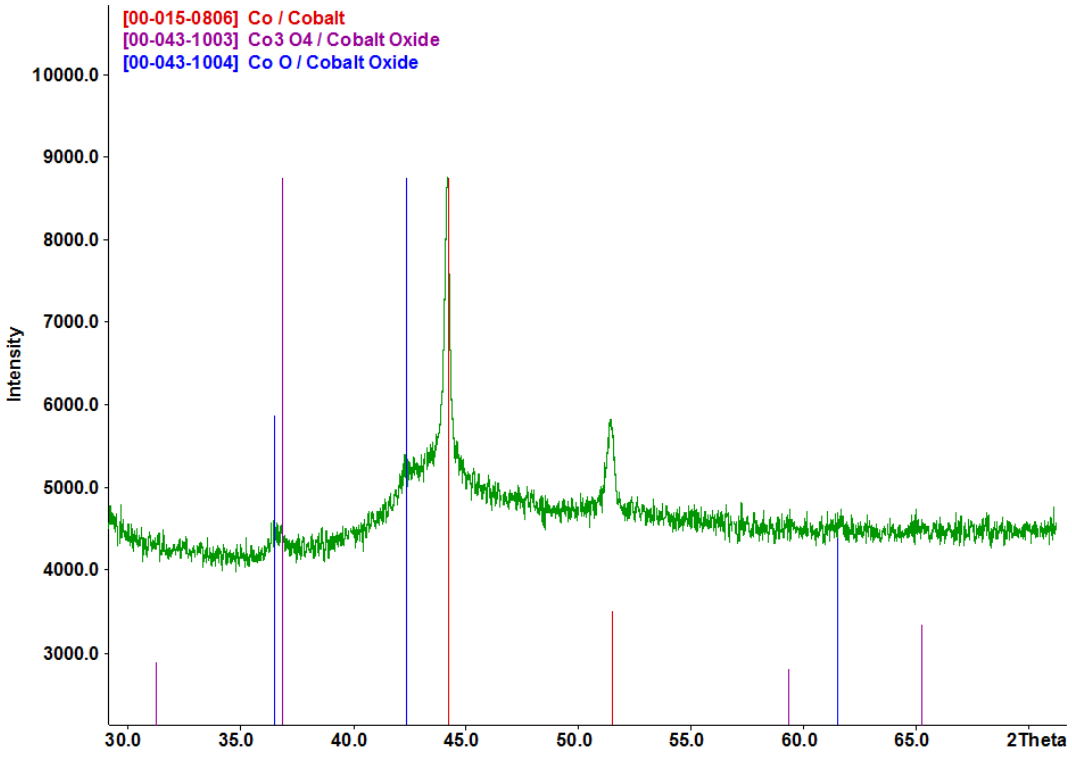

Fig. S7. XRD powder pattern of the active cobalt catalyst. The PDF (Powder Diffraction Files) numbers are in brackets.

S6. Procedure for catalyst recycling

100 mg Co_3O_4NGr/C catalyst (1 mol% Co) and 10 mL dry THF were added to oven dried pressure tube (ACE). Then, nitrobenzene (5 mmol) and HCOOH/Et_3N (5:2) mixture corresponds to 3.5 equiv. HCOOH and 250 μL n-hexadecane as internal standard were added sequentially. The pressure tube was flushed with argon, fitted with screw caps and the reactions were allowed progress at 100 for 13-15h After completion of the reaction, reaction mixture was cooled to room temperature. In each run catalyst was filtered off washed with THF and ethyl acetate. Filtrate containg reaction products was subjected GC-analysis. The fwashed catalyst was dryed and used for next run without any purifcation.

S7. NMR Data

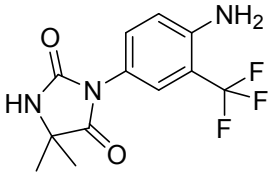

^{1}H NMR (300 MHz, $CDCl_3$) δ = 7.38 (d, *J*=2.4, 1H), 7.22 (dd, *J*=8.7, 2.4, 1H), 6.72 (d, *J*=8.7, 1H), 6.27 (s, 1H), 4.26 (s, 2H), 1.45 (s, 6H).

^{13}C NMR (75 MHz, DMSO-D_6) δ = 176.67, 154.57, 145.88, 131.93, 124.91 (d, J_{CF} = 5.25 Hz), 122.80 (d, J_{CF} = 5.25 Hz), 119.62, 116.70, 110.19 (d, J_{CF} = 3.48 Hz), 57.65, 24.64.

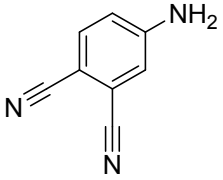

^{1}H NMR (300 MHz, $CDCl_3$) δ = 7.46 (d, *J*=8.6, 1H), 6.88 (d, *J*=2.4, 1H), 6.78 (dd, *J*=8.6, 2.4, 1H), 4.36 (s, 2H). ^{13}C NMR (101 MHz, DMSO-D_6) δ = 153.03, 134.89, 117.49, 117.22, 116.90, 116.41, 115.49, 97.78.

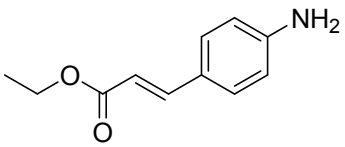

^{1}H NMR (300 MHz, $CDCl_3$) δ = 7.52 (d, *J*=15.9, 1H), 7.31 – 7.22 (m, 2H), 6.57 (d, *J*=8.5, 2H), 6.16 (d, *J*=15.9, 1H), 4.16 (q, *J*=7.1, 2H), 1.25 (t, *J*=7.1, 3H). ^{13}C NMR (75 MHz, $CDCl_3$) δ = 167.76, 148.59, 144.89, 129.89, 124.99, 124.78, 114.91, 113.73, 60.22, 14.43

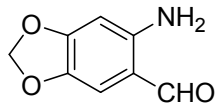

^{1}H NMR (300 MHz, $CDCl_3$) δ = 9.53 (s, 1H), 6.74 (s, 1H), 6.22 (s, 2H), 6.07 (s, 1H), 5.85 (s, 2H). ^{13}C NMR (75 MHz, $CDCl_3$) δ = 190.97, 154.02, 149.28, 139.41, 111.85, 111.55, 101.51, 95.99.

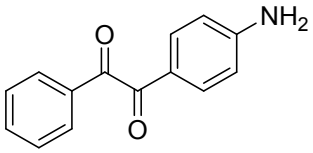

^{1}H NMR (300 MHz, $CDCl_3$) δ = 7.90 (d, *J*=9.8, 2H), 7.70 (d, *J*=9.2, 2H), 7.59 – 7.51 (m, 2H), 7.45 – 7.37 (m, 2H), 6.57 (d, *J*=8.8, 1H), 4.30 (s, 2H). ^{13}C NMR (75 MHz, DMSO-D_6) δ = 195.99, 191.70, 155.96, 134.84, 133.08, 133.01, 132.27, 129.28, 129.25, 119.64, 113.08.

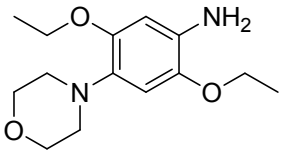

^{1}H NMR (300 MHz, $CDCl_3$) δ = 6.43 (s, 1H), 6.28 (s, 1H), 3.92 (dq, *J*=8.9, 7.0, 4H), 3.99 – 3.72 (m, 4H), 2.97 – 2.86 (m, 4H), 1.33 (td, *J*=7.0, 1.4, 6H). ^{13}C NMR (75 MHz, $CDCl_3$) δ = 146.55, 140.34, 132.81, 131.92, 105.47, 102.64, 67.40, 65.12, 64.24, 51.76, 15.25, 15.11.

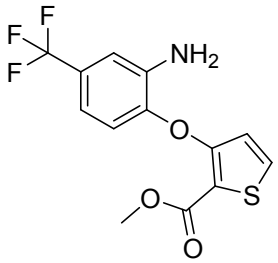

^{1}H NMR (300 MHz, $CDCl_3$) δ = 7.36 (d, *J*=5.5, 1H), 6.96 (s, 1H), 6.81 (d, *J*=4.3, 2H), 6.66 (d, *J*=5.5, 1H), 4.15 (s, 2H), 3.77 (s, 3H). ^{13}C NMR (75 MHz, DMSO-D_6) δ = 160.80, 156.81, 145.73, 140.10, 132.22, 129 (m), 122.55, 121.19, 118.12, 114.11, 112.48 (d, J_{CF} = 5.75 Hz), 112.38, (d, J_{CF} = 4.5 Hz), 111.41 (d, J_{CF} = 3.75 Hz), 51.77.

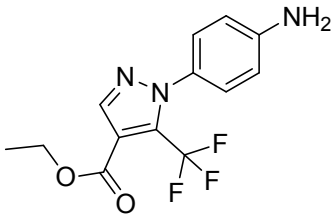

^{1}H NMR (300 MHz, $CDCl_3$) δ = 8.02 – 7.97 (m, 1H), 7.10 (d, *J* = 8.6, 2H), 6.65 – 6.61 (m, 2H), 4.29 (q, *J* = 7.1, 2H), 3.88 (s, 2H), 1.30 (t, *J* = 7.1, 3H). ^{13}C NMR (75 MHz, $CDCl_3$) δ = 161.24, 147.87, 142.05, 130.17, 126.96 (d, J_{CF} = 5.27 Hz), 121.00, 116.16, 114.66 (d, J_{CF} = 3.25 Hz), 112.43, 111.53 (d, J_{CF} = 5.25 Hz), 61.21, 14.14.

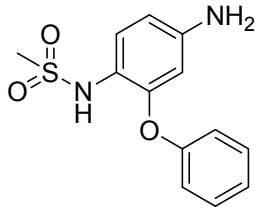

^{1}H NMR (300 MHz, $CDCl_3$) δ = 7.30 (t, *J*=8.0, 2H), 7.12 – 7.07 (m, 1H), 6.95 (s, 2H), 6.35 (d, *J*=8.6, 2H), 6.26 (s, 1H), 6.09 (s, 1H), 3.60 (s, 2H), 2.85 (s, 3H). ^{13}C NMR (75 MHz, $CDCl_3$) δ = 155.78, 151.04, 150.50, 146.07, 130.10, 126.96, 124.14, 118.91, 117.73, 110.61, 104.48, 38.96.

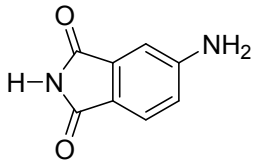

^{1}H NMR (400 MHz, DMSO-D_6) δ = 10.72 (s, 1H), 7.43 (d, *J*=8.2, 1H), 6.87 (d, *J*=2.0, 1H), 6.80 (dd, *J*=8.2, 2.1, 1H), 6.40 (s, 2H). ^{13}C NMR (101 MHz, DMSO-D_6) δ = 169.65, 169.32, 154.81, 135.43, 124.61, 117.88, 116.79, 106.59.

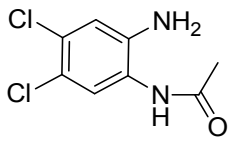

^{1}H NMR (400 MHz, DMSO-D_6) δ = 9.17 (s, 1H), 7.54 (s, 1H), 6.90 (s, 1H), 5.43 (m, 2H), 2.05 (s, 3H). ^{13}C NMR (101 MHz, DMSO-D_6) δ = 168.61, 141.79, 126.78, 125.57, 124.72, 123.39, 115.96, 115.55, 23.39.

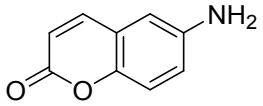

^{1}H NMR (300 MHz, DMSO-D_6) δ = 7.87 (d, *J*=9.5, 1H), 7.10 (d, *J*=8.8, 1H), 6.86 (dd, *J*=8.8, 2.7, 1H), 6.75 (d, *J*=2.8, 1H), 6.35 (d, *J*=9.5, 1H), 5.26 (s, 2H). ^{13}C NMR (75 MHz, DMSO-D_6) δ = 160.48, 145.56, 145.13, 144.34, 119.06, 118.70, 116.54, 115.81, 110.16.

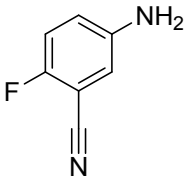

^{1}H NMR (300 MHz, $CDCl_3$) δ = 7.01 – 6.81 (m, 1H), 6.84 – 6.68 (m, 2H), 3.70 (s, 2H). ^{13}C NMR (75 MHz, $CDCl_3$) δ = 158.16, 154.87, 143.19 (d, J_{CF} = 2.25 Hz), 121.19 (d, J_{CF} = 7.5 Hz), 117.41 (d, J_{CF} = 29.25 Hz), 116.94, 114.45, 101.2 (d, J_{CF} = 16.5 Hz).

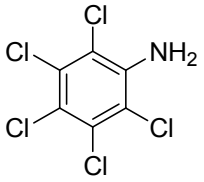

^{1}H NMR (300 MHz, $CDCl_3$) δ = 4.68 (s, 2H). ^{13}C NMR (101 MHz, DMSO-D_6) δ = 142.46, 129.96, 116.87, 115.49.

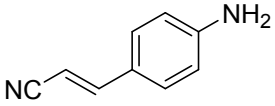

^{1}H NMR (300 MHz, $CDCl_3$) δ = 7.19 – 7.16 (m, 3H), 6.56 (d, *J*=8.6, 2H), 5.53 (d, *J*=16.6, 1H), 3.97 (s, 2H). ^{13}C NMR (101 MHz, DMSO-D6) δ = 151.95, 150.89, 133.42, 129.57, 121.22, 114.85, 113.73, 112.78.

8. References

[S1] J. Casanovas, J.M. Ricart, J. Rubio, E. Illas, J.M. Jiménez-Mateos, *J. Am. Chem. Soc.* **1996**, *118,* 8071-8076.

[S2] J.R. Pels, F. Kapteijn, J.A. Moulijn, Q. Zhu, K.M. Thomas, *Carbon*, **1995**, *33,* 1641-1653.

[S3] W. Grünert, R. Feldhaus, K. Anders, E.S. Shipiro, G.V. Antoshin, K.M. Minachev, *J. Electron. Spectrosc. Relat. Phenom.* **1986**, *40*, 187-192.

[S4] M.C. Biesinger, B.P. Payne, A.P. Grosvenor,L.W.M Lau, A.R. Gerson, R. S.C. Smart, *Appl.Surf.Sci.,* **2011,** 257, 2717

[S5] S. Angelov, E. Zhecheva, R. Stoyanova, M. Atanasov, *J. Phys. Chem. Solids,* **1990,** *51,* 1157.

[S6] P. Dutta, M.S. Seehra, K. Thota, J. Kumar,*J. Phys.: Condens. Matter*, **2008**, *20,* 15218

[S7] A. Brückner, A. Martin, N. Steinfeldt, G.-U. Wolf, B. Lücke, *J. Chem. Soc. Faraday Trans.* **1996,** *92,* 4257-4263.

[S8] U.D. Wdowik, D. Legut, *J. Phys. Chem. Solids,* **2008,** *69,* 1698-1703.

[S9] F.C. Campbel, "Elements of metallurgy and engineering alloys", Materials Park, Ohio: ASM International 2008, Chapter 29, p. 557.

S9 NMR Spectra

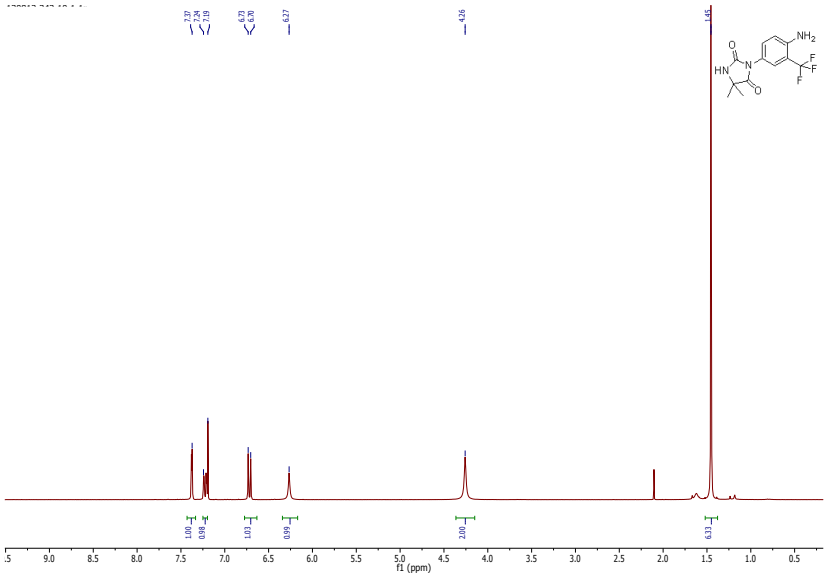

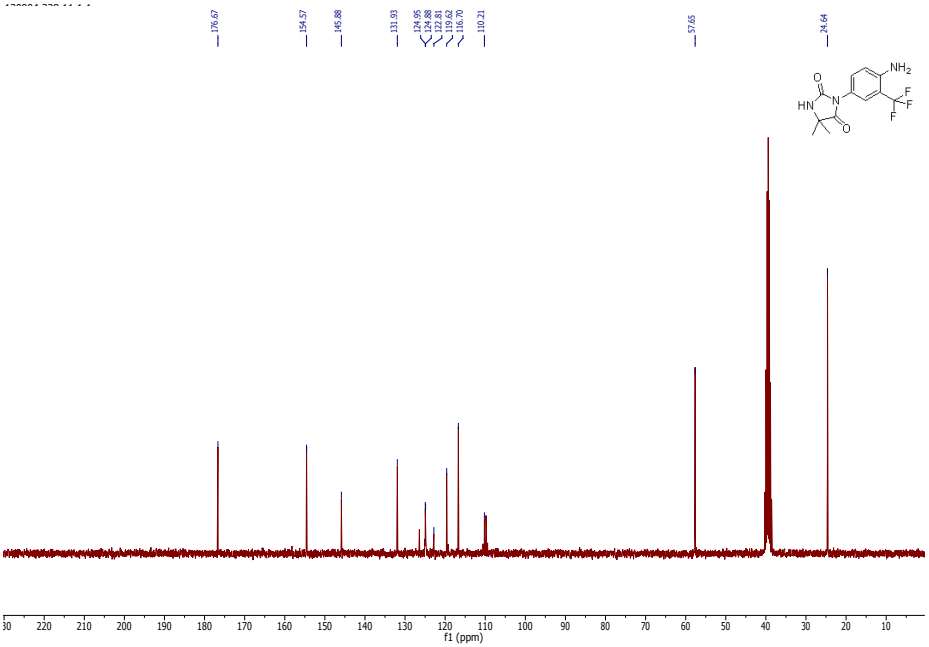

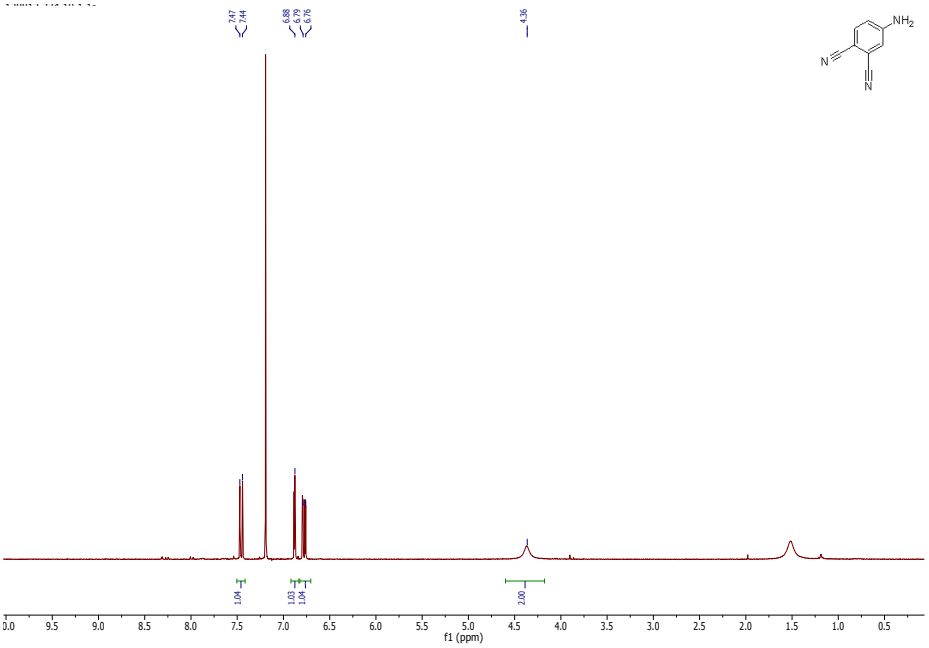
7.47
7.44
6.88
6.79
6.76
4.36
NH2
N
N
1.04
1.03
1.04
2.00
f1 (ppm)

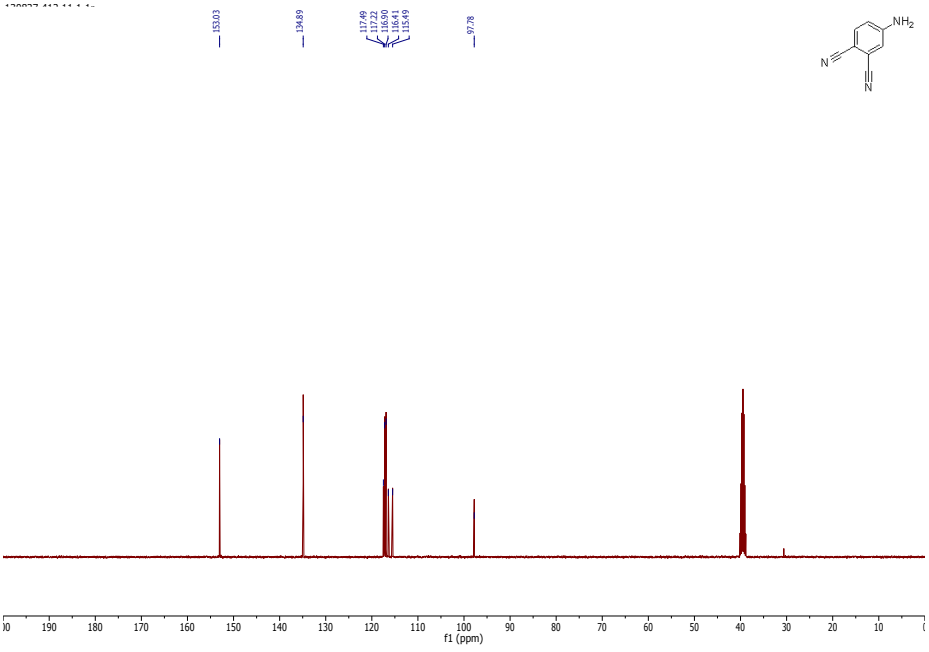
153.03
134.89
117.49
117.22
116.90
116.41
115.49
97.78
NH2
N
N
f1 (ppm)

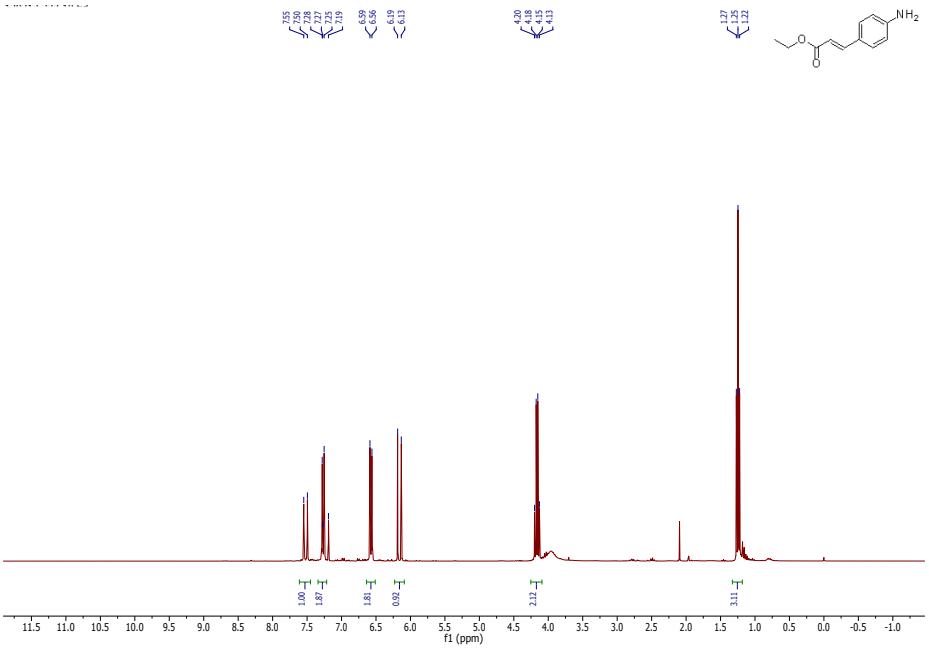
7.55
7.50
7.28
7.27
7.25
7.19
6.59
6.56
6.19
6.13
4.20
4.18
4.15
4.13
1.27
1.25
1.22
NH2
O
O
1.00
1.87
1.81
0.92
2.12
3.11
11.5 11.0 10.5 10.0 9.5 9.0 8.5 8.0 7.5 7.0 6.5 6.0 5.5 5.0 4.5 4.0 3.5 3.0 2.5 2.0 1.5 1.0 0.5 0.0 -0.5 -1.0
f1 (ppm)

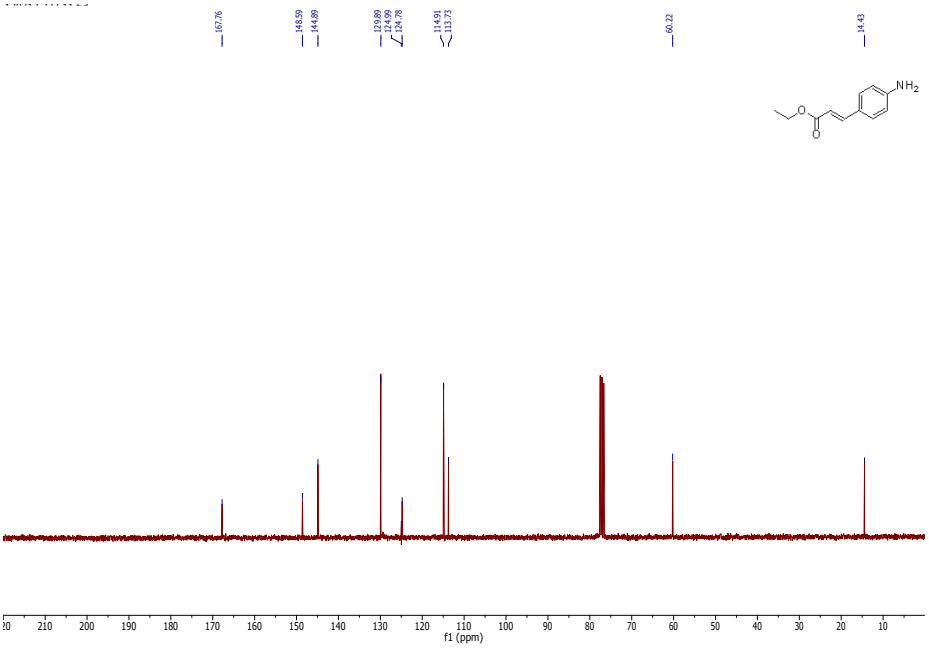
167.76
148.59
144.89
129.89
124.99
124.78
114.91
113.73
60.22
14.43
NH2
O
O
210 200 190 180 170 160 150 140 130 120 110 100 90 80 70 60 50 40 30 20 10
f1 (ppm)

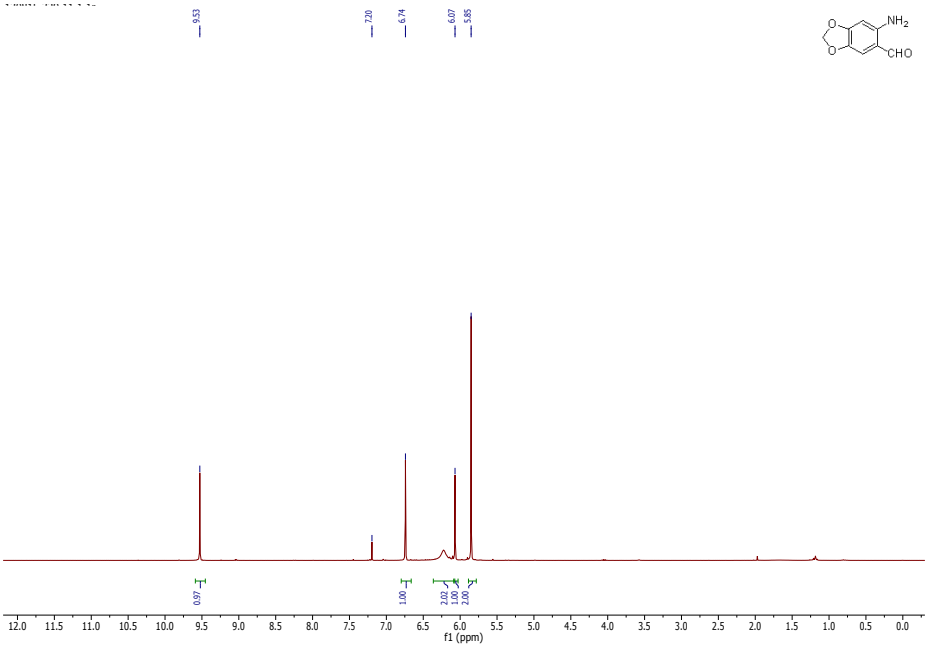
9.53
7.20
6.74
6.07
5.85
NH2
CHO
0.97
1.00
2.02
1.00
2.00
12.0 11.5 11.0 10.5 10.0 9.5 9.0 8.5 8.0 7.5 7.0 6.5 6.0 5.5 5.0 4.5 4.0 3.5 3.0 2.5 2.0 1.5 1.0 0.5 0.0
f1 (ppm)

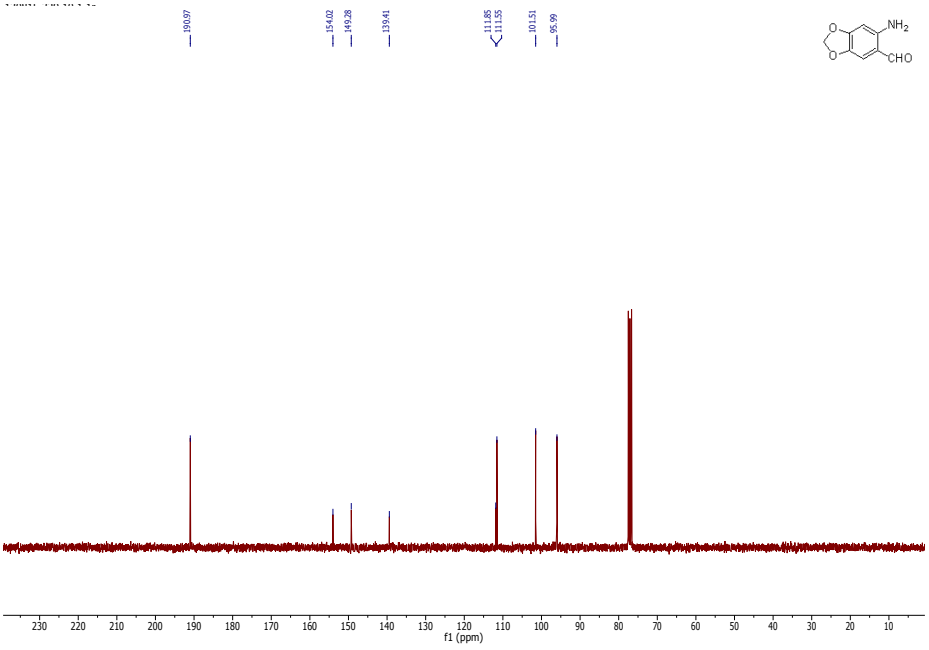
190.97
154.02
149.28
139.41
111.85
111.55
101.51
95.99
NH2
CHO
230 220 210 200 190 180 170 160 150 140 130 120 110 100 90 80 70 60 50 40 30 20 10
f1 (ppm)

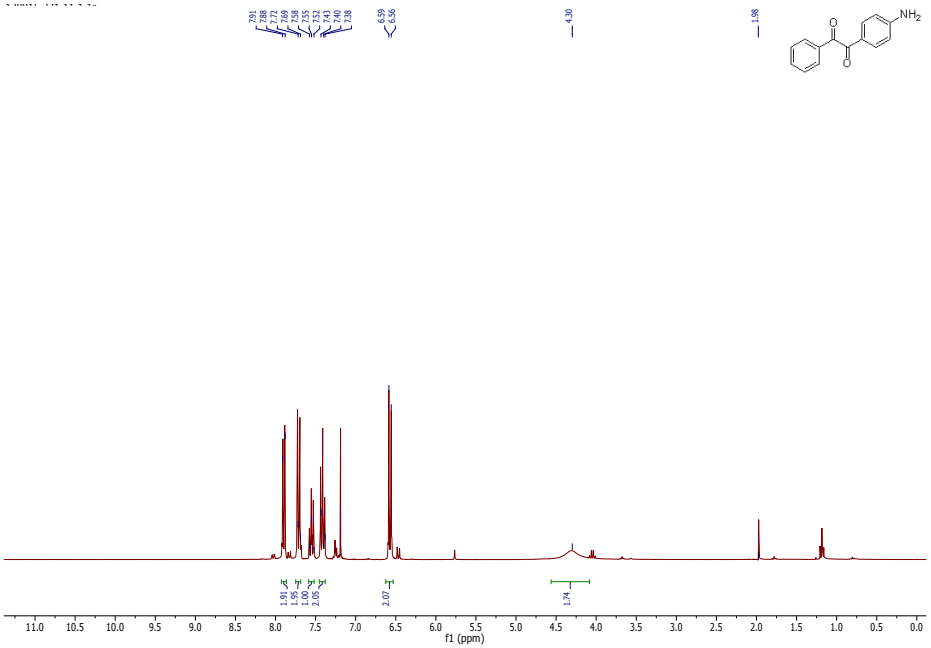
7.91
7.88
7.73
7.69
7.58
7.55
7.53
7.43
7.40
7.38
6.59
6.56
4.30
1.98
NH2
1.91
1.95
1.00
2.05
2.07
1.74
f1 (ppm)

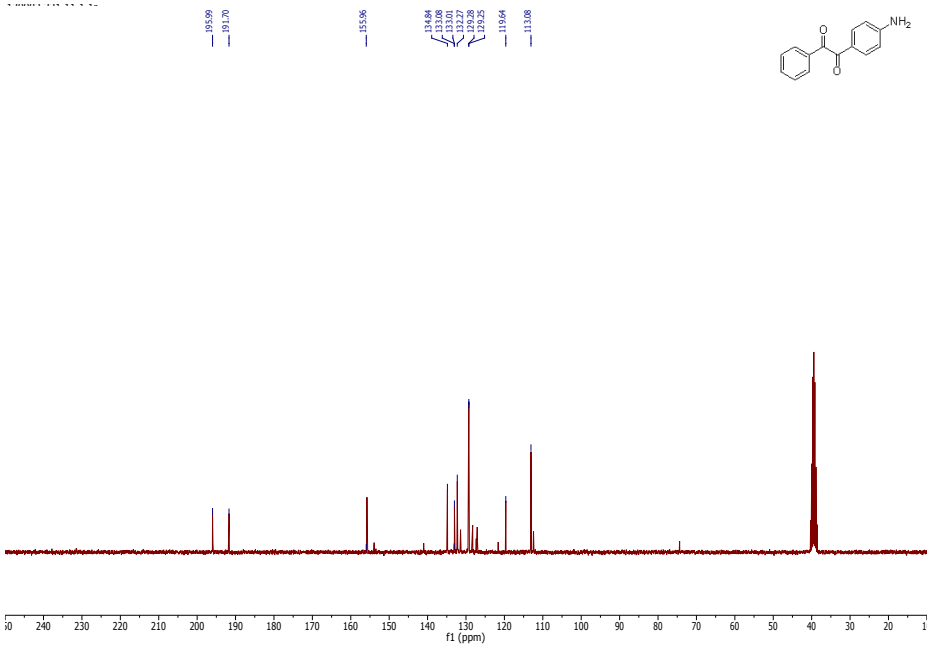
195.99
191.70
155.96
134.84
133.08
133.01
132.27
129.28
129.25
119.64
113.08
NH2
f1 (ppm)

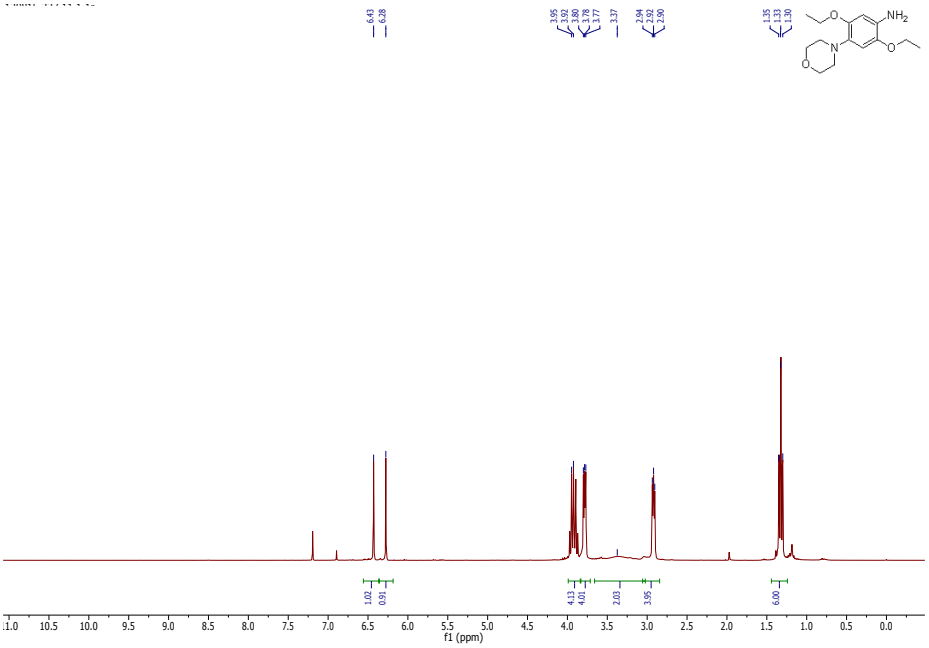
6.43
6.28
3.95
3.92
3.80
3.78
3.77
3.37
2.94
2.92
2.90
1.35
1.33
1.30
NH2
O
N
O
O
1.02
0.91
4.13
4.01
2.03
3.95
6.00
f1 (ppm)

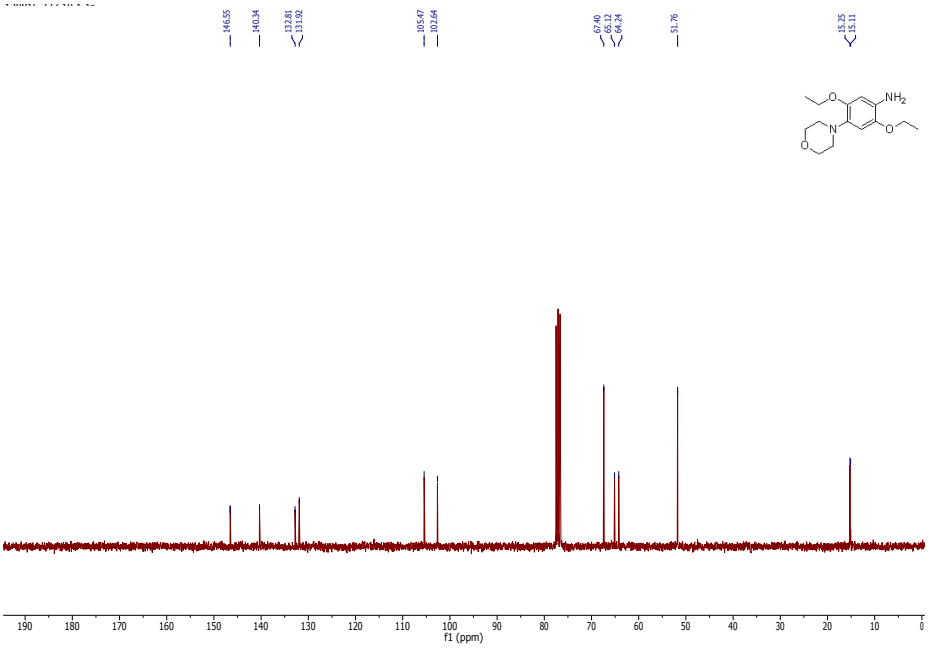
146.55
140.34
132.81
131.92
105.47
102.64
67.40
65.73
64.24
51.76
15.25
15.11
NH2
O
N
O
O
f1 (ppm)

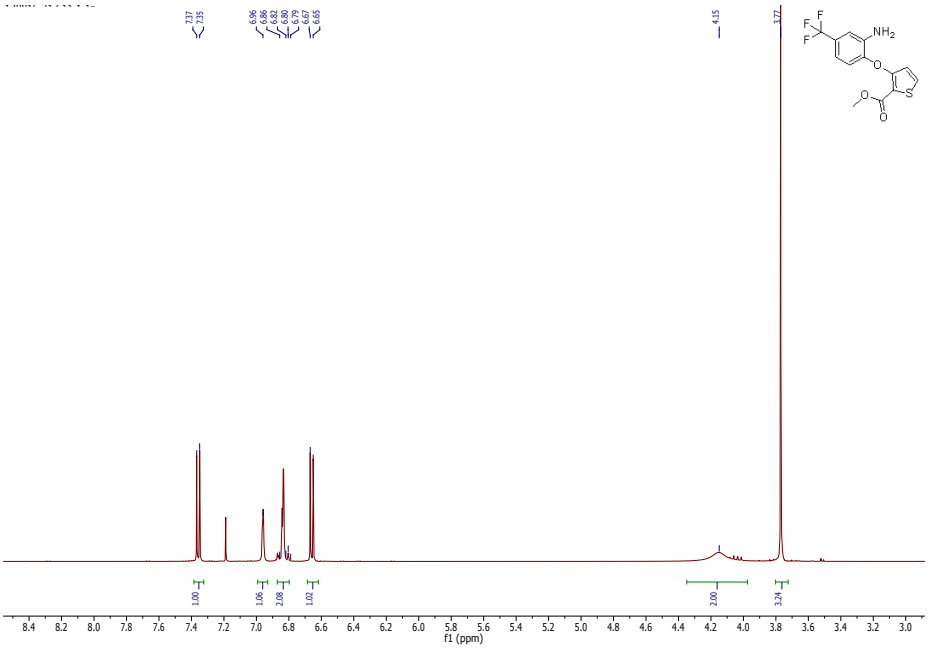
7.37
7.35
6.96
6.86
6.82
6.80
6.79
6.67
6.65
4.15
3.77
1.00
1.06
2.08
1.02
2.00
3.24
f1 (ppm)

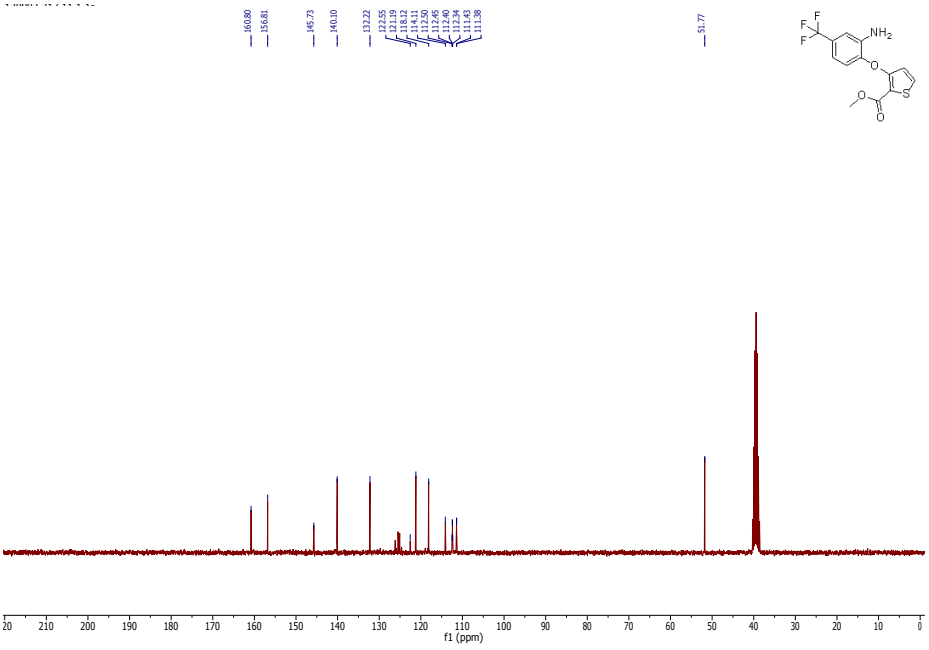
160.80
156.81
145.73
140.10
132.22
122.55
121.19
118.12
114.41
113.50
112.45
112.40
112.24
111.45
111.38
51.77
f1 (ppm)

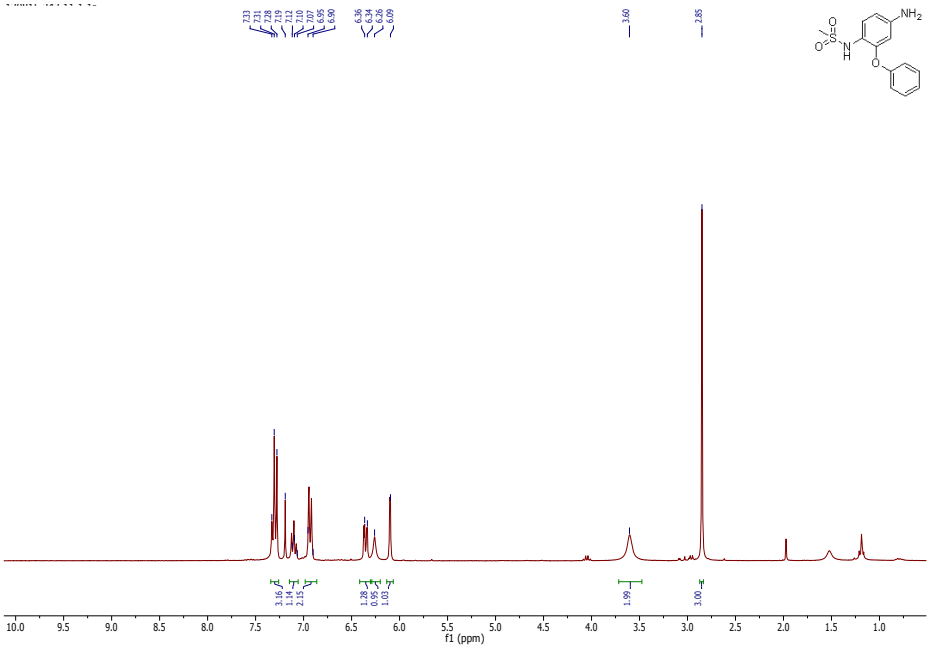
7.33
7.31
7.28
7.19
7.12
7.10
7.07
6.95
6.90
6.36
6.34
6.26
6.09
3.60
2.85
NH2
3.16
1.14
2.15
1.28
0.95
1.03
1.99
3.00
10.0 9.5 9.0 8.5 8.0 7.5 7.0 6.5 6.0 5.5 5.0 4.5 4.0 3.5 3.0 2.5 2.0 1.5 1.0
f1 (ppm)

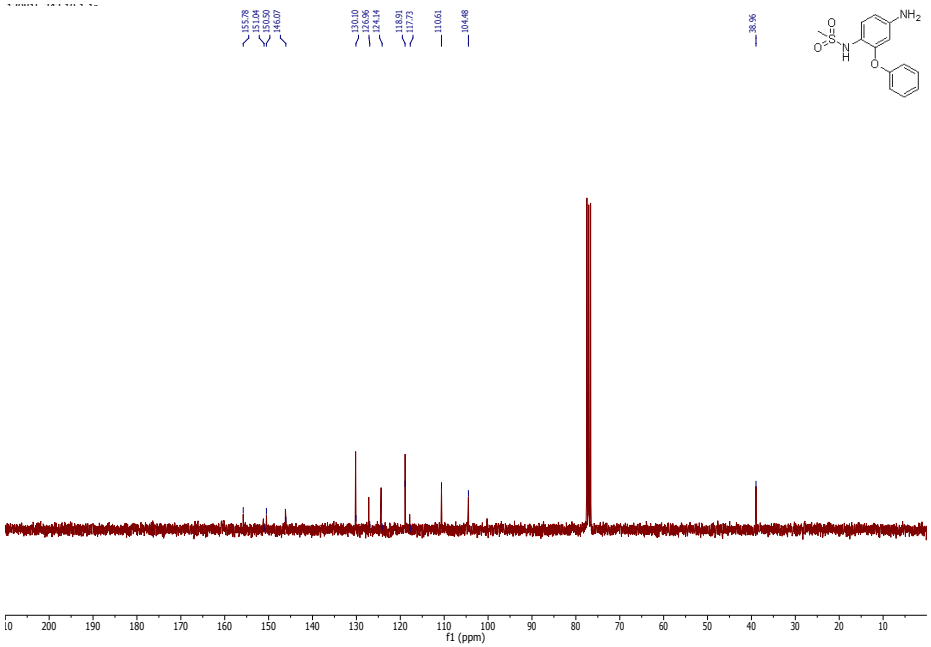
155.78
151.04
150.50
146.07
130.10
126.96
124.14
118.91
117.73
110.61
104.48
38.96
NH2
200 190 180 170 160 150 140 130 120 110 100 90 80 70 60 50 40 30 20 10
f1 (ppm)

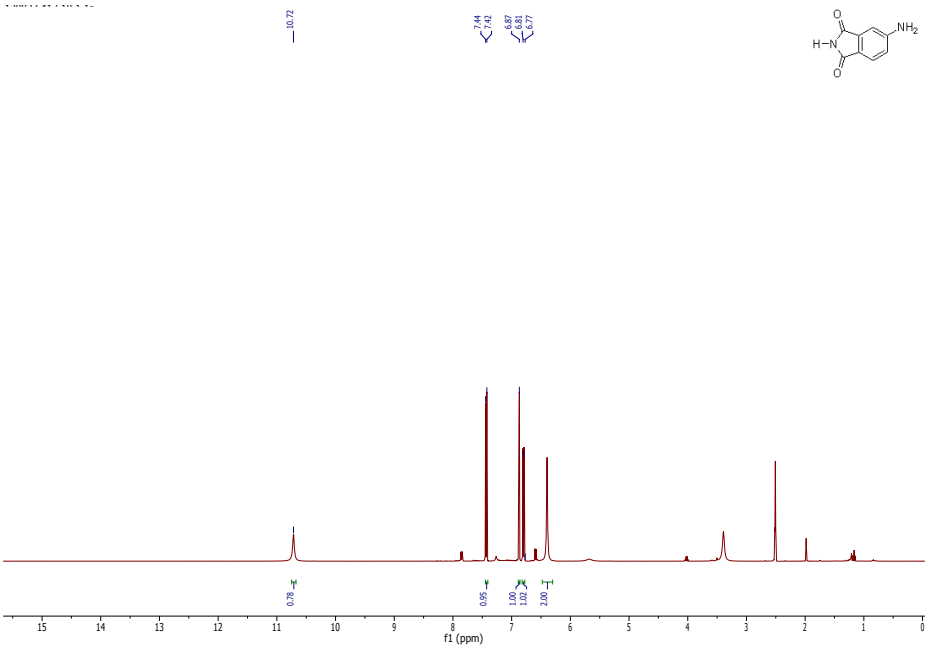
10.72
7.44
7.42
6.87
6.81
6.77
NH2
0.78
0.95
1.00
1.02
2.00
f1 (ppm)

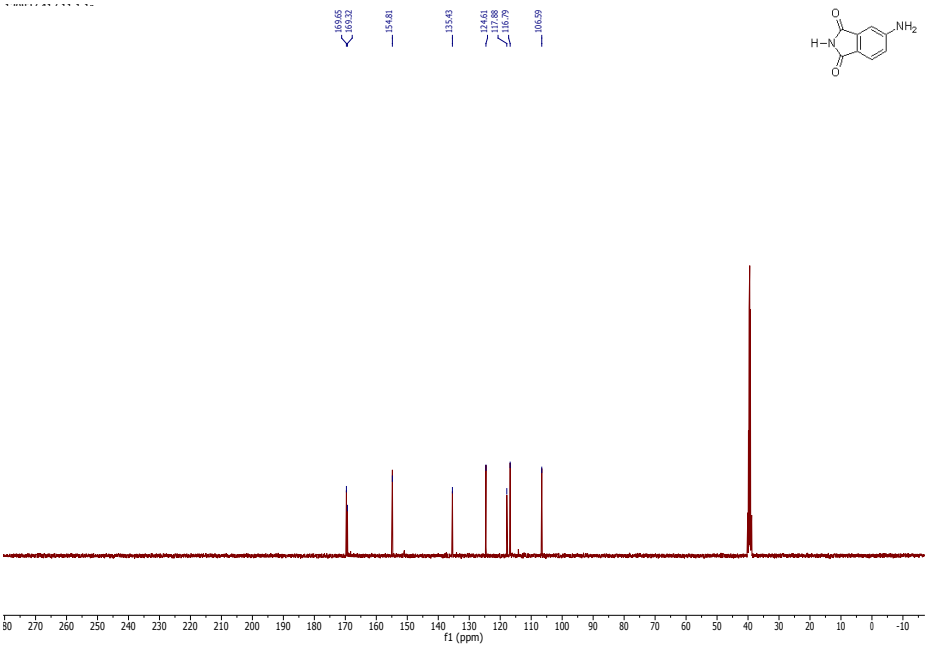
169.65
169.32
154.81
135.43
124.61
117.88
116.79
106.59
NH2
f1 (ppm)

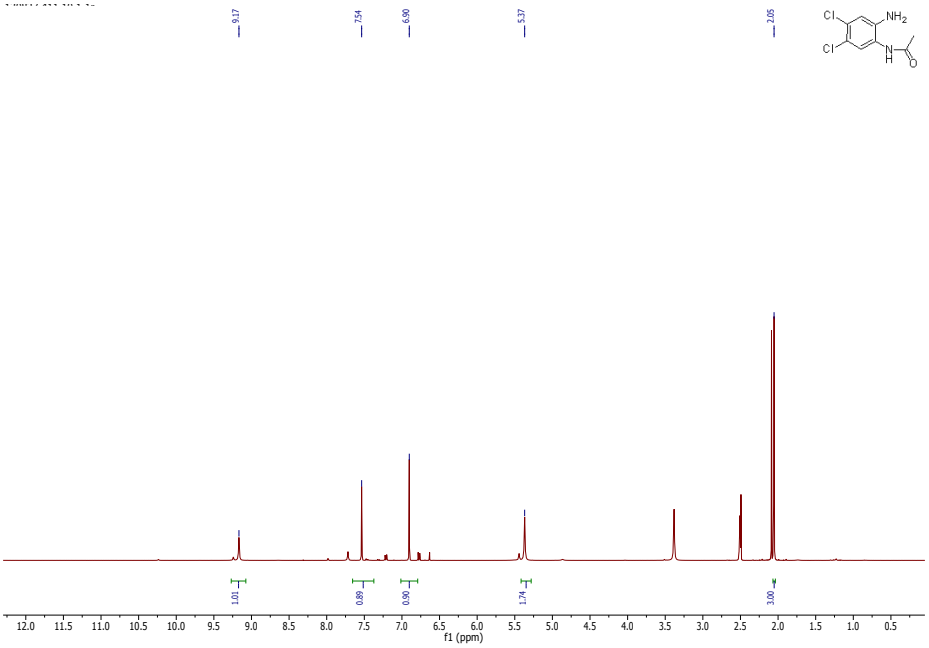
9.17
7.54
6.90
5.37
2.05
Cl
Cl
NH2
N
H
O
1.01
0.89
0.90
1.74
3.00
f1 (ppm)

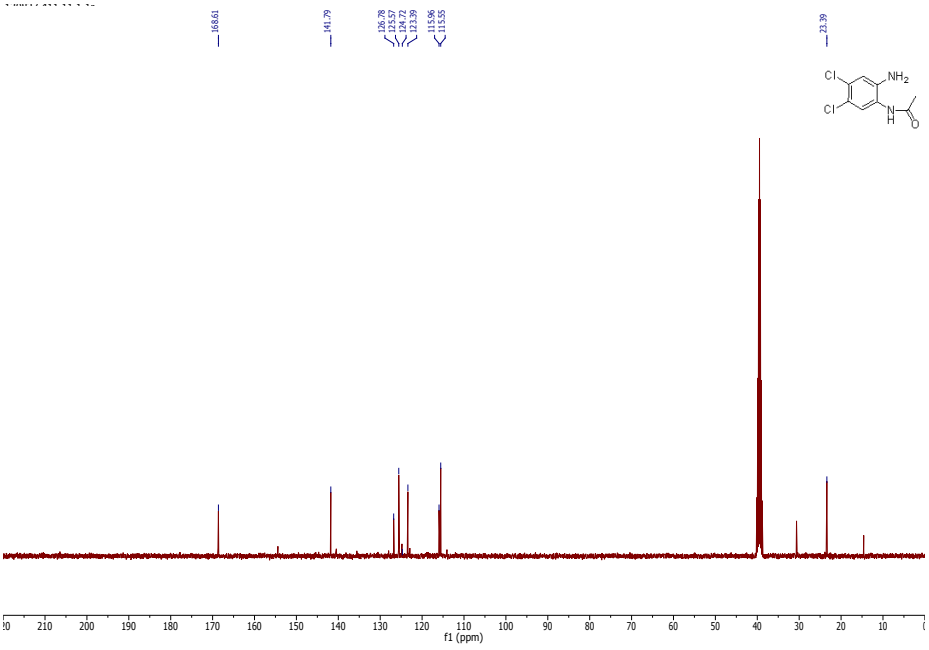
168.61
141.39
126.78
125.57
124.72
123.39
115.96
115.55
23.39
Cl
Cl
NH2
N
H
O
f1 (ppm)

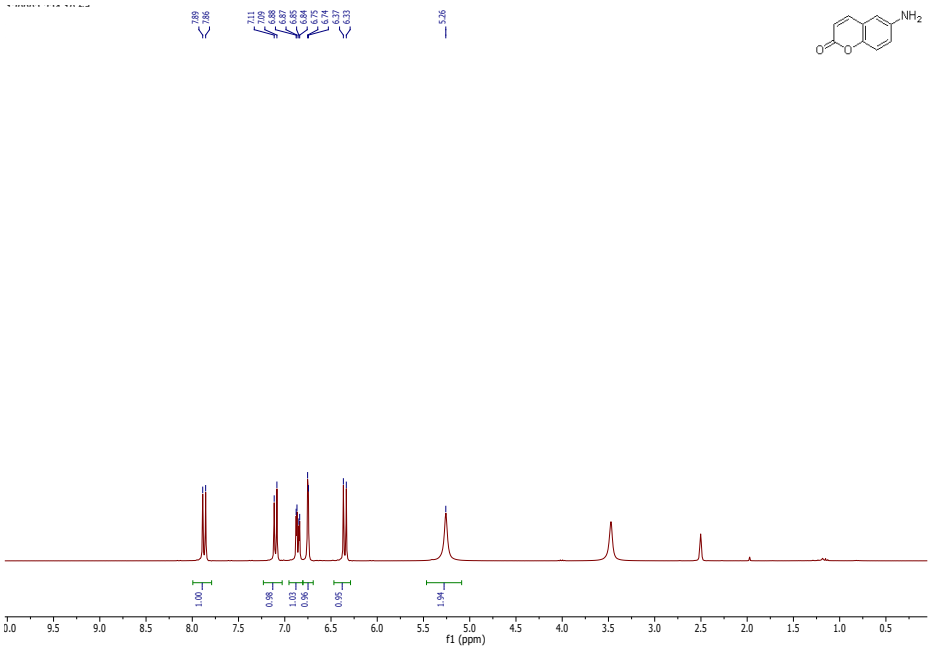
7.89
7.86
7.11
7.09
6.88
6.87
6.85
6.84
6.75
6.74
6.37
6.33
5.26
NH2
O
O
1.00
0.98
1.03
0.96
0.95
1.94
f1 (ppm)

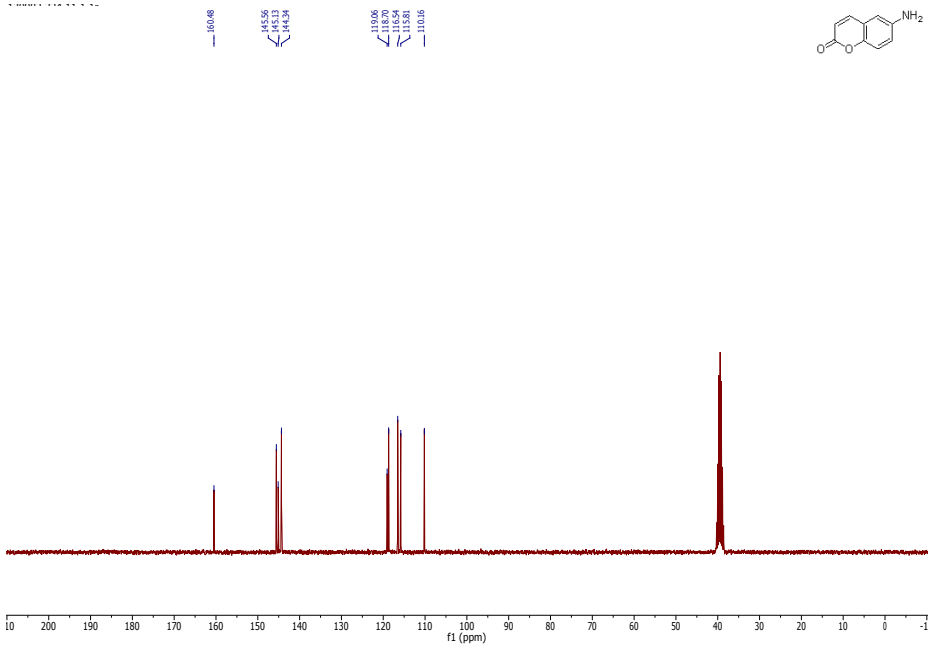
160.48
145.56
145.13
144.34
119.06
118.70
116.54
115.81
110.16
NH2
O
O
f1 (ppm)

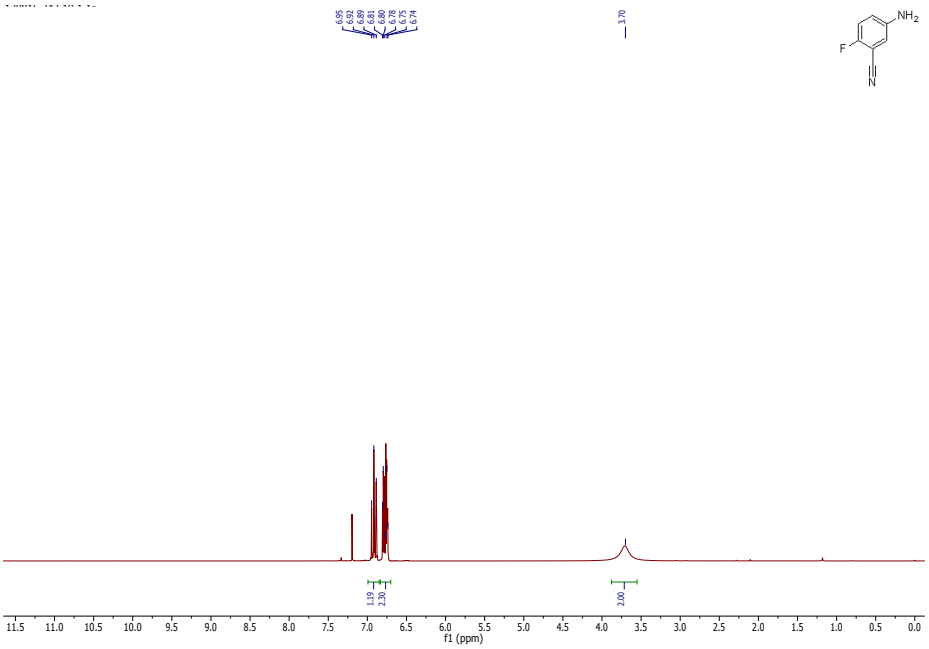
6.95
6.92
6.89
6.81
6.80
6.78
6.75
6.74
3.70
NH2
F
N
1.19
2.30
2.00
11.5 11.0 10.5 10.0 9.5 9.0 8.5 8.0 7.5 7.0 6.5 6.0 5.5 5.0 4.5 4.0 3.5 3.0 2.5 2.0 1.5 1.0 0.5 0.0
f1 (ppm)

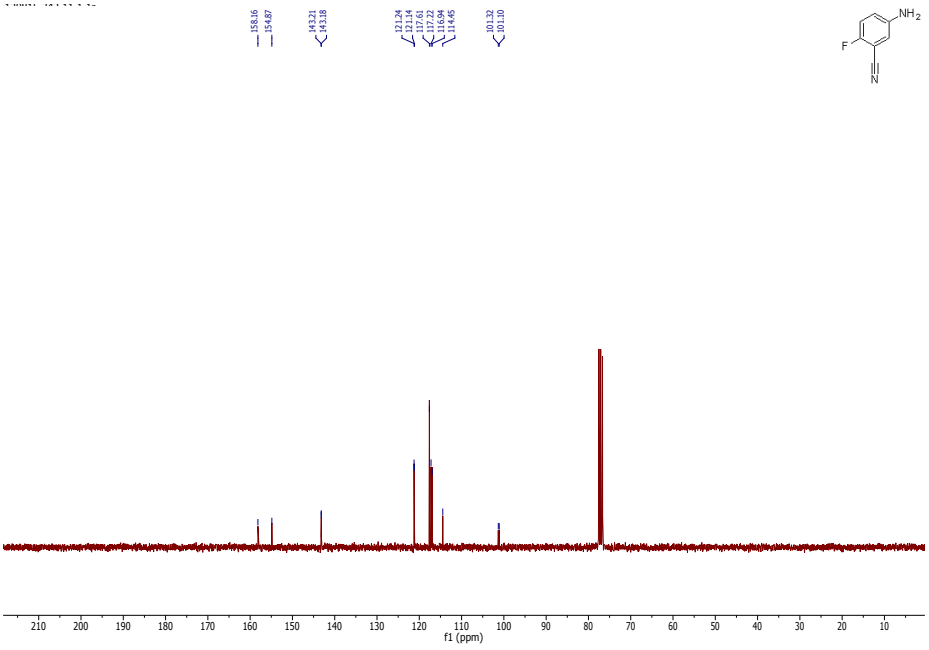
158.16
154.87
143.21
143.18
121.24
121.14
117.61
117.22
116.94
116.45
101.32
101.10
NH2
F
N
210 200 190 180 170 160 150 140 130 120 110 100 90 80 70 60 50 40 30 20 10
f1 (ppm)

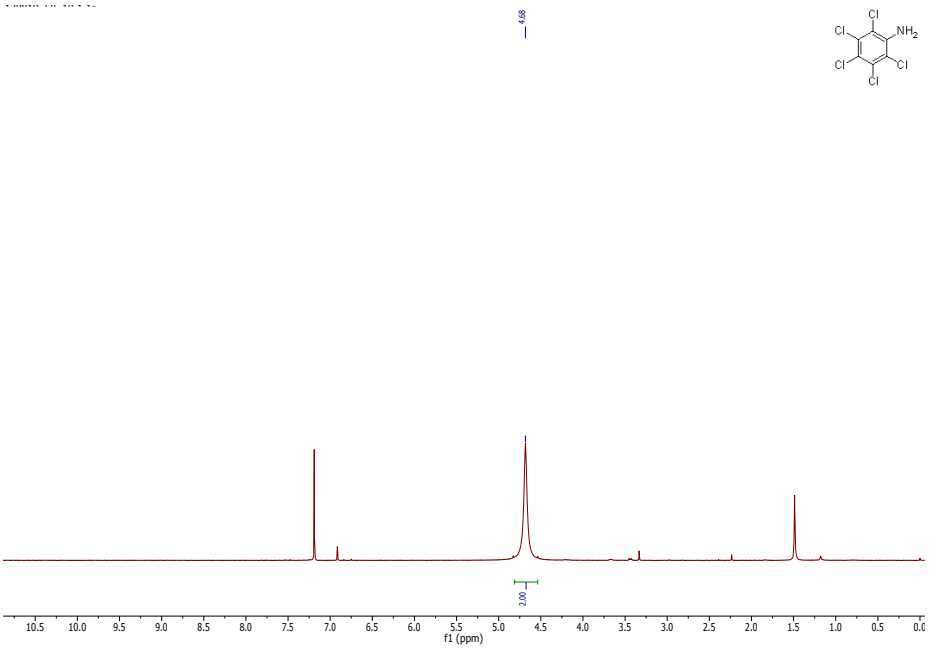
4.68
Cl
NH2
Cl
Cl
Cl
Cl
2.00
10.5 10.0 9.5 9.0 8.5 8.0 7.5 7.0 6.5 6.0 5.5 5.0 4.5 4.0 3.5 3.0 2.5 2.0 1.5 1.0 0.5 0.0
f1 (ppm)

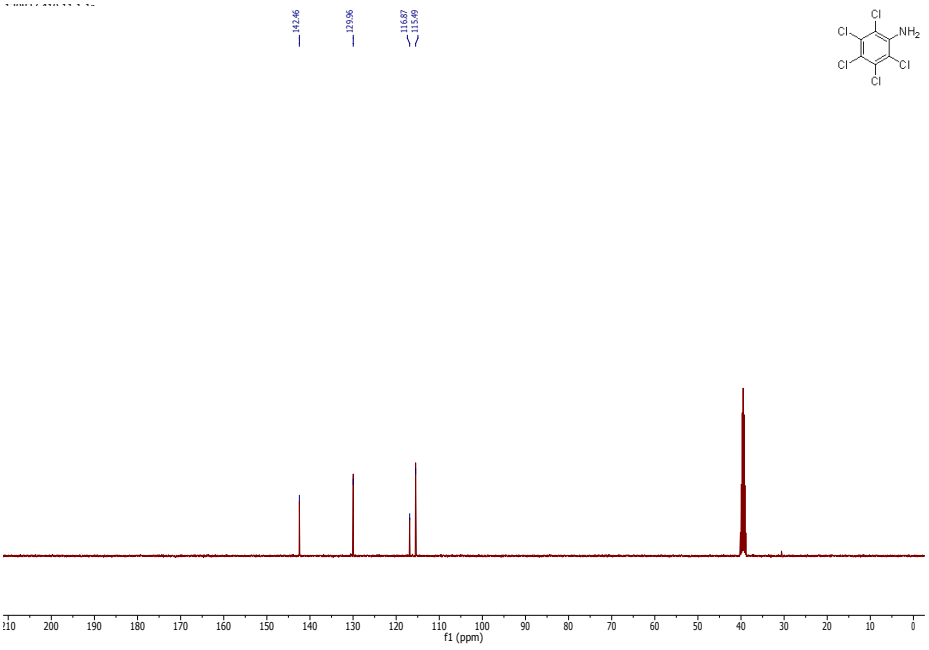
142.46
129.96
116.87
115.49
Cl
NH2
Cl
Cl
Cl
Cl
210 200 190 180 170 160 150 140 130 120 110 100 90 80 70 60 50 40 30 20 10 0
f1 (ppm)

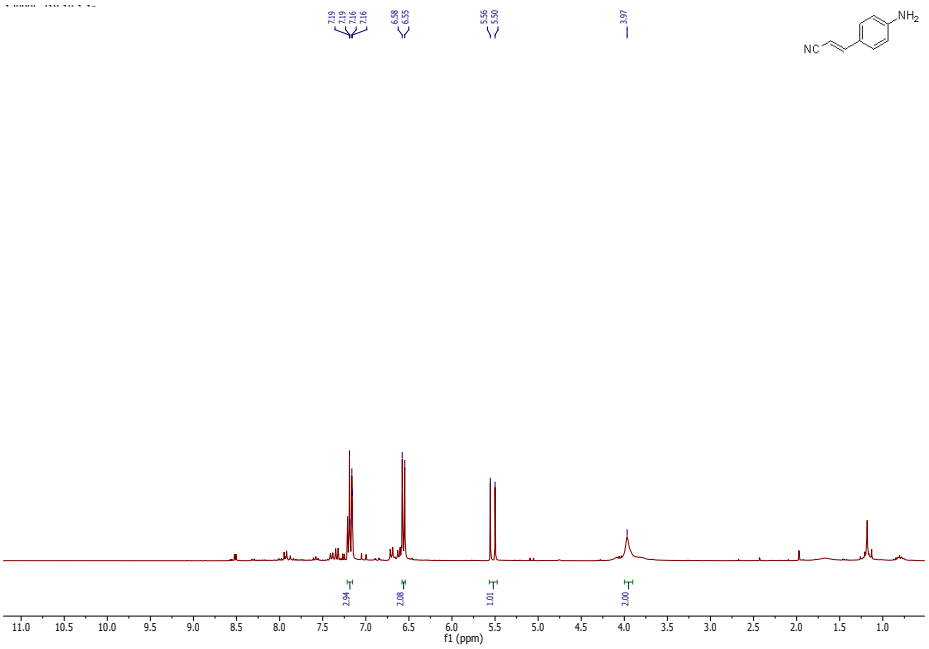
7.19
7.18
7.16
7.16
6.38
6.35
5.56
5.50
3.97
NH2
NC
2.94
2.08
1.01
2.00
11.0
10.5
10.0
9.5
9.0
8.5
8.0
7.5
7.0
6.5
6.0
5.5
5.0
4.5
4.0
3.5
3.0
2.5
2.0
1.5
1.0
f1 (ppm)

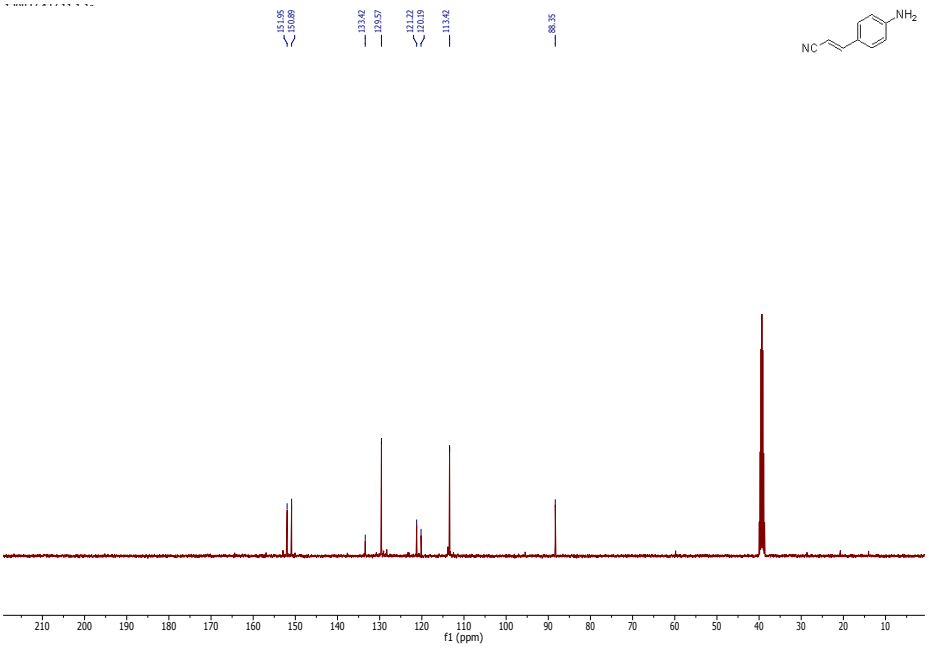
151.95
150.89
133.42
129.57
121.22
120.19
113.42
88.35
NH2
NC
210
200
190
180
170
160
150
140
130
120
110
100
90
80
70
60
50
40
30
20
10
f1 (ppm)